WAVES: THE RADIO AND PLASMA WAVE INVESTIGATION ON THE WIND SPACECRAFT

J.-L. BOUGERET
DESPA-URA CNRS 264, Observatoire de Paris-Meudon, France

M. L. KAISER
NASA/Goddard Space Flight Center, Greenbelt, Maryland, U.S.A.

P. J. KELLOGG
School of Physics and Astronomy, University of Minnesota, Minneapolis, U.S.A.

R. MANNING
DESPA-URA CNRS 264, Observatoire de Paris-Meudon, France

K. GOETZ and S. J. MONSON
School of Physics and Astronomy, University of Minnesota, Minneapolis, U.S.A.

N. MONGE
DESPA-URA CNRS 264, Observatoire de Paris-Meudon, France

L. FRIEL
DESPA-URA CNRS 264 and STIL, Maynooth, Ireland

C. A. MEETRE
NASA/GSFC and Hughes STX, Lanham, Maryland, U.S.A.

and

C. PERCHE, L. SITRUK and S. HOANG
DESPA-URA CNRS 264, Observatoire de Paris-Meudon, France

(Received 27 October, 1993)

Abstract. The WAVES investigation on the WIND spacecraft will provide comprehensive measurements of the radio and plasma wave phenomena which occur in Geospace. Analyses of these measurements, in coordination with the other onboard plasma, energetic particles, and field measurements will help us understand the kinetic processes that are important in the solar wind and in key boundary regions of the Geospace. These processes are then to be interpreted in conjunction with results from the other ISTP spacecraft in order to discern the measurements and parameters for mass, momentum, and energy flow throughout geospace. This investigation will also contribute to observations of radio waves emitted in regions where the solar wind is accelerated. The WAVES investigation comprises several innovations in this kind of instrumentation: among which the first use, to our knowledge, of neural networks in real-time on board a scientific spacecraft to analyze data and command observation modes, and the first use of a wavelet transform-like analysis in real time to perform a spectral analysis of a broad band signal.

1. Investigation Objectives

The goal of the WAVES investigation on the WIND spacecraft is to provide comprehensive coverage of radio and plasma wave phenomena in the frequency range from a fraction of a Hertz up to about 14 MHz for the electric field and 3 kHz for the magnetic field. This package will permit several kind of measurements, all of

Space Science Reviews **71:** 231–263, 1995.

which are essential to understanding the Earth's environment – Geospace – and its response to varying solar wind conditions. The WIND orbit will have an apogee as large as 250 earth radii and a perigee of at least 5 earth radii. It is described in more detail in this issue and will permit observations in the solar wind and through key boundary regions of the Geospace. The spacecraft will spin at 20 revolutions per minute. We briefly describe below how the WAVES measurements will contribute to both large scale, global analyses and small scale analyses.

1.1. PLASMA PHYSICS

In situ measurements of different modes of plasma waves will give information on local processes and couplings in different regions and boundaries of the Geospace leading to plasma instabilities: magneto-acoustic waves, ion cyclotron waves, whistler waves, electron plasma oscillations, electron burst noise (Lacombe *et al.*, 1985; Canu, 1990) and other types of electrostatic or electromagnetic waves.

The Time Domain Sampler (TDS) of the WAVES investigation is designed to continue the study of dissipation processes in plasmas, beyond those begun by our team 's URAP-FES experiment on Ulysses (Stone *et al.*, 1992). These processes are particularly important in plasma boundaries such as the bow shock. There are extensive, but conflicting (strong, weak turbulence) theories of the dissipation of Langmuir waves through parametric decay, soliton formation, collapse, and dissipation to electron tails. The WIND TDS will have sufficient time resolution to resolve the waveform of most Langmuir waves, and to study their evolution statistically.

Fluctuations and turbulence in the solar wind are an important subject which is not well understood. The WAVES FFT receiver will allow measurement of the complete spectrum of magnetic fluctuations in its frequency range, and identification of the modes, through the phases between the various components.

1.2. IN SITU ELECTRON DIAGNOSIS FROM THERMAL NOISE ANALYSIS

In situ plasma spectroscopy of the thermal noise spectrum will permit a determination of the electron density and temperature. This technique has been extensively used on ICE and ULYSSES, for both solar wind analyses and encounters - comet Giacobini-Zinner, planet Jupiter- (Meyer-Vernet and Perche, 1989). It requires a well calibrated, very sensitive instrument. The WAVES Thermal Noise Receiver (TNR) will cover an electron density range from less than 1 cm^{-3} to about 500 cm^{-3} and an electron temperature range from about 10^3 K to more than 10^6 K. It will allow rapid measurements of plasma density fluctuations (every 1.5 s or half spacecraft spin).

1.3. Remote Sensing of the Earth's Magnetosphere

Remote sensing of radio waves generated in the Earth's environment in a large spectrum of frequencies will allow us to cover a broad range of phenomena, including Auroral Kilometric Radiation (AKR) (Gurnett, 1974), Non Thermal Continuum (NTC) (Gurnett, 1975), Isotropic Terrestrial Kilometric Radiation (ITKR) (Steinberg *et al.*, 1990), radio waves at the plasma frequency (Burgess *et al.*, 1987) or its harmonic (Lacombe *et al.*, 1988) produced upstream of the bow shock by shock-accelerated or reflected electrons.

1.4. Remote Sensing of the Interplanetary Medium

Shocks and energetic particle streams will be tracked from about 3–4 solar radii from the center of the Sun through about 1 AU (astronomical unit). The spinning spacecraft technique will be used to determine several source parameters including the direction of the source centroid, the source diameter and polarization (Manning and Fainberg, 1980; Fainberg *et al.*, 1985). Similar techniques have been extensively utilized by similar investigations on the ICE and ULYSSES spacecraft (Hoang *et al.*, 1994; Reiner *et al.*, 1993). In particular, the little explored 1–14 MHz range (up to the ionospheric cutoff) will be covered by a specific radio receiver. This is the range where most of the solar wind acceleration takes place. We believe that most large interplanetary shocks form within this range, and that they are likely to accelerate particles. Both shock waves and energetic particle events can be remotely tracked by their associated radio emissions. In the same frequency range, storms of mildly energetic electrons, continuously ejected from solar active regions (Bougeret *et al.*, 1984) may help us understand the acceleration of the slow solar wind (Bougeret *et al.*, 1983). Radio observations from about 30 MHz and up to more than 500 MHz will be provided by ground-based instruments including the ARTEMIS radio telescope and spectrograph (Maroulis *et al.*, 1993), which will be located at the Greek Centre of Space Communications (Thermopiles Station), in Greece and operated by the University of Athens. This overall frequency coverage will provide, for the first time, a comprehensive monitoring of radio phenomena from the base of the solar corona up to the orbit of the Earth.

2. Instrument Overview

The WAVES instrument is a joint effort of the Paris-Meudon Observatory, the University of Minnesota, and the Goddard Space Flight Center.

A block diagram of the WAVES instrument is shown in Figure 1. The sensors are:

(1) three electric dipolar antenna systems supplied by Fairchild Space (two are coplanar, orthogonal wire dipole antennas in the spin-plane, the other a rigid spin-axis dipole) and

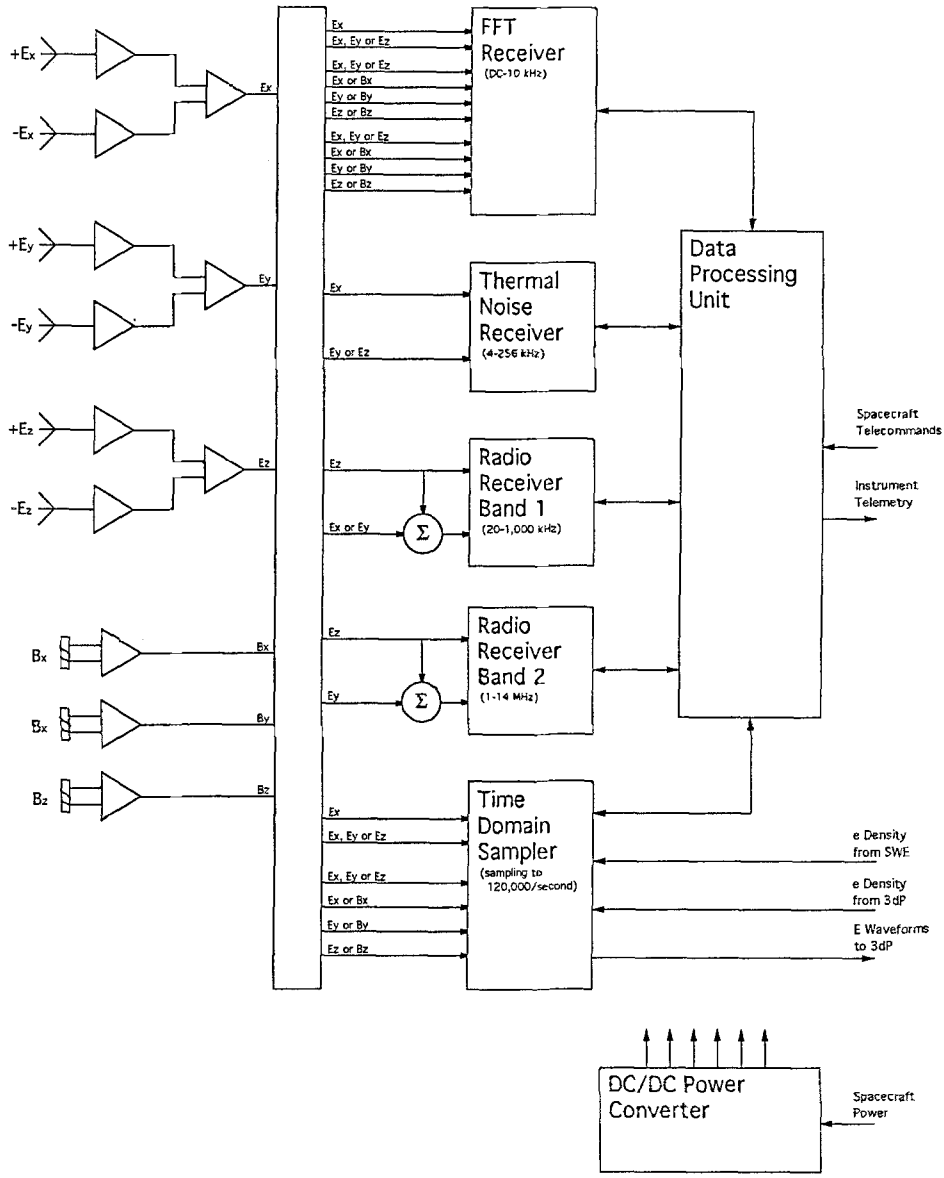

Fig. 1. WIND/WAVES overall block diagram.

(2) three magnetic search coils mounted orthogonally (designed and built by the University of Iowa).

After preamplification, the sensor outputs are routed to the analysis electronics, consisting of a low frequency (DC – 10 kHz) FFT receiver, a broadband (4–256 kHz) multi-channel analyzer designed principally to study the electron thermal

noise, two dual radio receivers covering the band 20 kHz to 13.825 MHz, and a time-domain waveform sampler (sampling to 120 000 s^{-1}).

The experiment is controlled by a central data processing unit (DPU) which will be used in flight to reconfigure the sensor outputs and to maximize the science return for the bit rate and power allotments that are available. A DC/DC power converter is also part of the electronics stack. The frequency ranges of the five subsystems are shown in Figure 2, together with the main science objectives. The ground segment ARTEMIS is shown as RAD3 on this Figure. The principal characteristics of the analysis electronics are summarized in Table I. In this table the spin-plane electric antennas are referred to as E_x and E_y, the axial electric antenna as E_z and the 3 search coil magnetic axes as B_x, B_y, and B_z.

3. Instrumentation

The instrument comprises six antenna units (supplied by Fairchild Space), plus six preamplifiers, three magnetic search coils mounted orthogonally, with their preamplifiers (designed and built by the University of Iowa), and two electronics stacks grouping together the hardware developed at Meudon and Minnesota respectively: stack 1 (WAVES1) for RAD1, RAD2, TNR and the power converter, stack 2 (WAVES2) for FFT, TDS and the DPU. Table II gives the physical characteristics of the instrument.

The total primary power is 28 W. The efficiency of the power converter is 68%.

3.1. Sensors

There are two orthogonal electric dipoles which are deployed after launch in the plane of spin of the spacecraft. They are of the motor-driven wire type. The stable position of the antennas is determined by centrifugal force. The two dipoles are of different lengths. The longer one, designated E_x, is 100 m tip-to-tip. The length of the shorter dipole (E_y) is 15 m tip-to-tip. These lengths are limited by the upper observation frequency of the RAD1 and RAD2 receivers, respectively.

The spin-axis dipole (E_z) will be deployed along the spin-axis of the spacecraft. Because of stability considerations on a rotating spacecraft, the antenna must be as stiff as possible. The antenna is of the motor-driven flexible extended tube type and about 12 m long tip-to-tip.

The triaxial magnetic search coil, and its preamplifiers, are similar to those developed for the POLAR spacecraft.

3.2. Preamplifiers

The preamplifiers for the electric antennas are located very close to the base of each antenna deployment mechanism. This is required to minimize the effect of

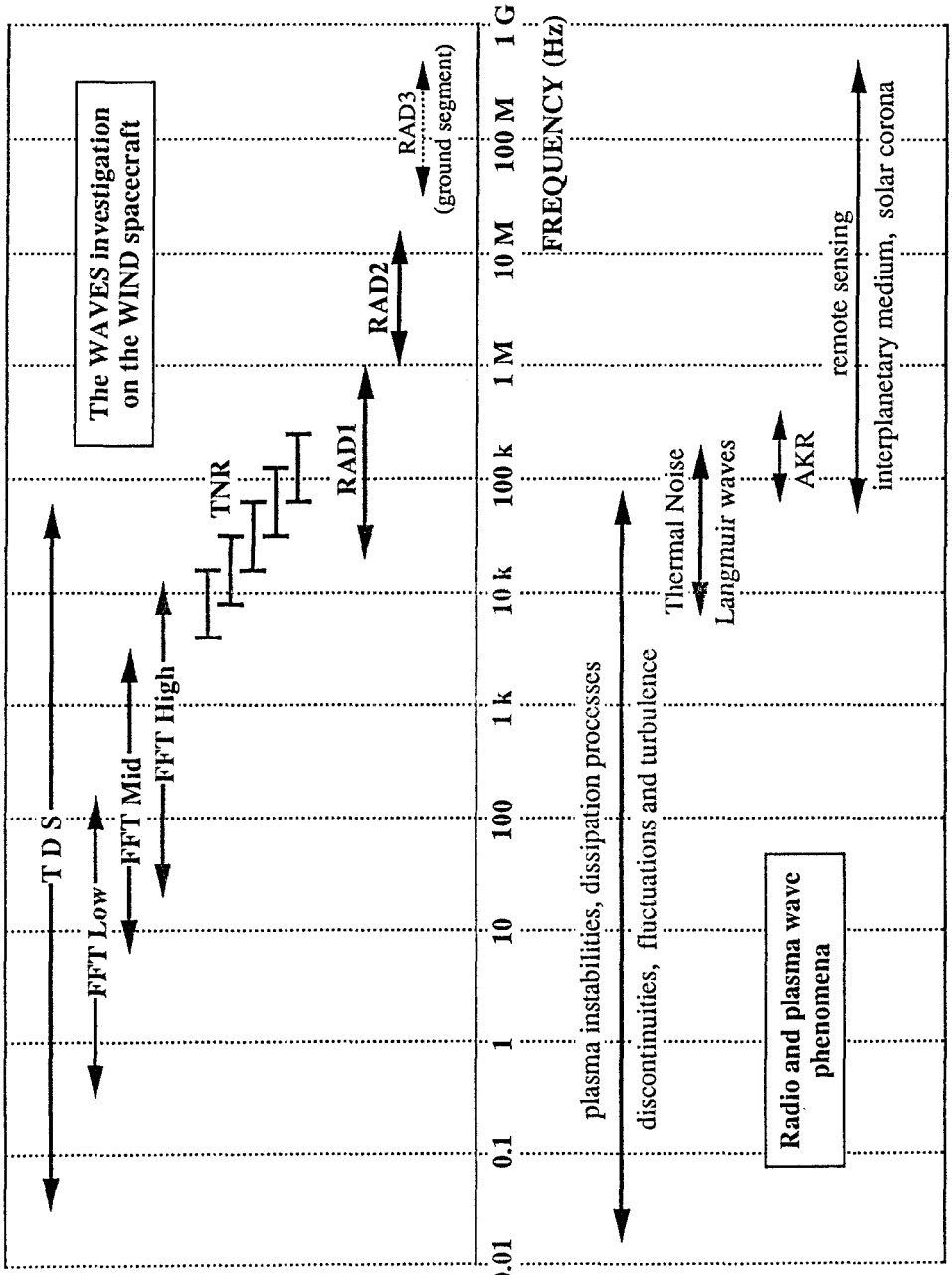

Fig. 2. Frequency coverage of the WAVES investigation. FFT and TDS analyze both the electric field and the magnetic field. TNR and the RADs analyze the electric field only.

TABLE I

Principal characteristics of the waves electronics

1. Low frequency FFT receiver (FFT)	
Low band	
Inputs	4 of E_x, E_y, E_z, B_x, B_y or B_z
Frequency range	0.3–170 Hz
No. channels	4
Sensitivity	250 μV (r.m.s.)
Dynamic range	72 dB
Mid band	
Inputs	4 of E_x, E_y, E_z, B_x, B_y or B_z
Frequency range	5.5 Hz–2.275 kHz
No. channels	4
Sensitivity	10 μV (r.m.s.)
Dynamic range	110 dB
High band	
Inputs	2 of E_x, E_y or E_z
Frequency range	22 Hz–11 kHz
No. channels	2
Sensitivity	1 μV (r.m.s.)
Dynamic range	128 dB
2. Thermal noise receiver (TNR)	
Inputs	E_x, E_y or E_z
Frequency range	4–256 kHz
No. channels	32 or 16 per band (5 bands)
Bandwidth	400 Hz–6.4 kHz
Sensitivity	7 nV/sqrt (Hz)
3. Radio receiver band 1 (RAD1)	
Inputs	$E_x + E_z$, E_z
Frequency range	20–1040 kHz
No. channels	256
Bandwidth	3 kHz
Sensitivity	7 nV/sqrt (Hz)
4. Radio receiver band 2 (RAD2)	
Inputs	$E_t + E_z$, E_z
Frequency range	1.075–13.825 MHz
No. channels	256
Bandwidth	20 kHz
Sensitivity	7 nV/sqrt (Hz)
5. Time domain sampler (TDS)	
Fast sampler	
Inputs	2 of E_x, E_y or E_z
Sample rate	up to 120 ksamples per second per channel
Memory	1 Mbits
Sensitivity	80 μV (r.m.s.)
Dynamic range	90 dB
Slow Sampler	
Inputs	4 of E_x, E_y, E_z, B_x, B_y, or B_z
Sample rate	up to 7.5 ksamples per second per channel
Memory	1 Mbits
Sensitivity	300 μV (r.m.s.)
Dynamic range	90 dB

TABLE II
Physical characteristics of the waves instrument

	Mass/unit (kg)	Number of units	Total mass (kg)	Dimensions per unit (l×L×h) (mm)
Sensors:				
wire boom mechanisms				
– 2 × 50 m	3.45	2	6.9	430 × 190 × 183
– 2 × 7.5 m 3.35	2	6.7	430 × 190 × 183	
axial boom mechanisms	6.5	2	13.0	509 × 172 × 222
search coil	0.3	3	0.9	406 × 38 × 37
	subtotal for sensors		27.5	
Electronics:				
– preamps	0.2	6	1.2	77 × 112 × 36
– WAVES1		1	5.8	179 × 222 × 201
– WAVES2		1	8 7	234 × 222 × 319
	subtotal for electronics		15.7	

the base capacity, which can severely limit the sensitivity of the experiment. Each preamplifier has three outputs: one with near unity gain for the RAD2 higher frequency portion of the instrument, another with gain shared by the TNR, RAD1, RAD2, FFT, and TDS receivers, and one with unity gain for the TDS and DC part of the instrument.

3.3. FFT RECEIVER (FFT)

The low-frequency FFT receiver contains a microprocessor-controlled FFT (Fast Fourier Transform) processor (Figure 3). The low frequency spectrum is divided into three frequency bands, high (22 Hz to 11 kHz), medium (5 Hz to 2.7 kHz) and low (.3 Hz to 170 Hz). The low band is synchronized to the spin rate of the spacecraft.

Each channel of the FFT is passed through an anti-aliasing low-pass filter corresponding to the channel frequency range and then digitized with a large dynamic range. The analog to digital conversion is performed using a floating point conversion technique which allows the greatest dynamic range. Each sample in the high and mid frequency bands has a 12 bit mantissa and a 2-bit exponent which gives a theoretical dynamic range of 144 dB. The actual dynamic range is given in Table I. The samples from the low frequency band are 12 bit samples giving a dynamic range of 72 dB.

After collecting a time series of 1024 samples on each channel of a particular band, the time series is windowed and a standard FFT is produced by a specialized

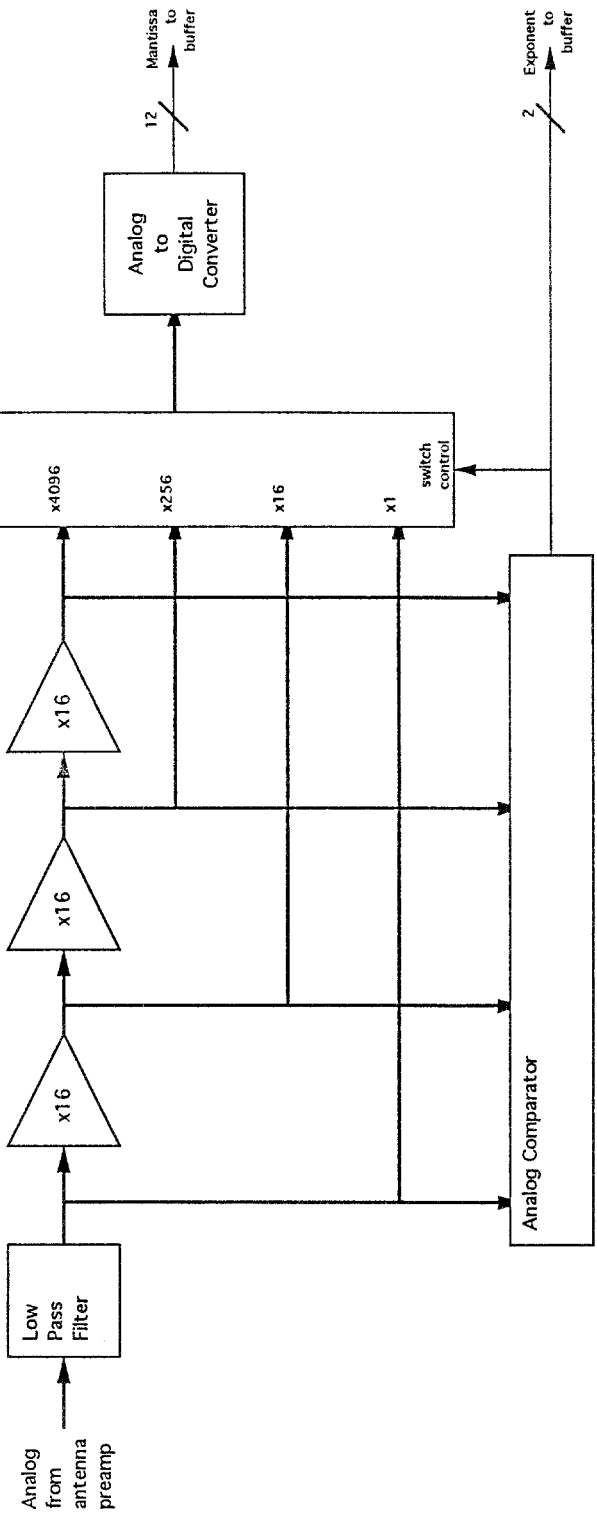

Fig. 3a. The FFT receiver. 144 dB 'floating point' analog do digital converter (used in high- and mid-frequency channels).

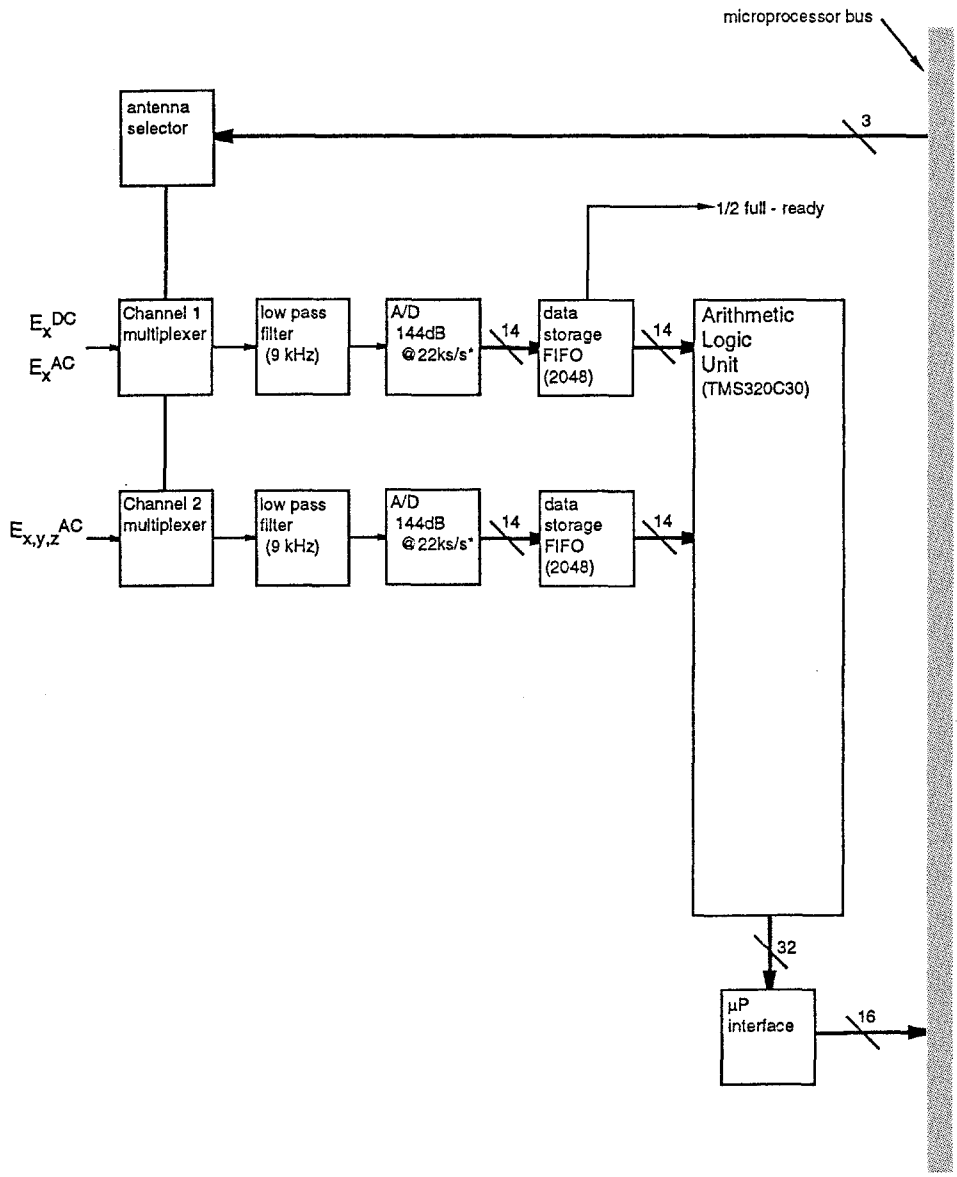

* sample rate = spin rate (spins/second) * 8 (sectors/spin) * 8 (FFT/sector) * 1024 (samples/FFT) + ε = 22,000 samples/second

Fig. 3b. The FFT receiver. High band digitizers.

floating point digital signal processor. This high performance DSP allows the 1024 point floating point transform to be completed in as little as 3 ms. The power spectrum is then converted to have logarithmic frequency spacing with 3–4 frequencies per octave, completed by averaging the FFT components in frequency space. Each such spectrum is further averaged over some number of spacecraft rotations with

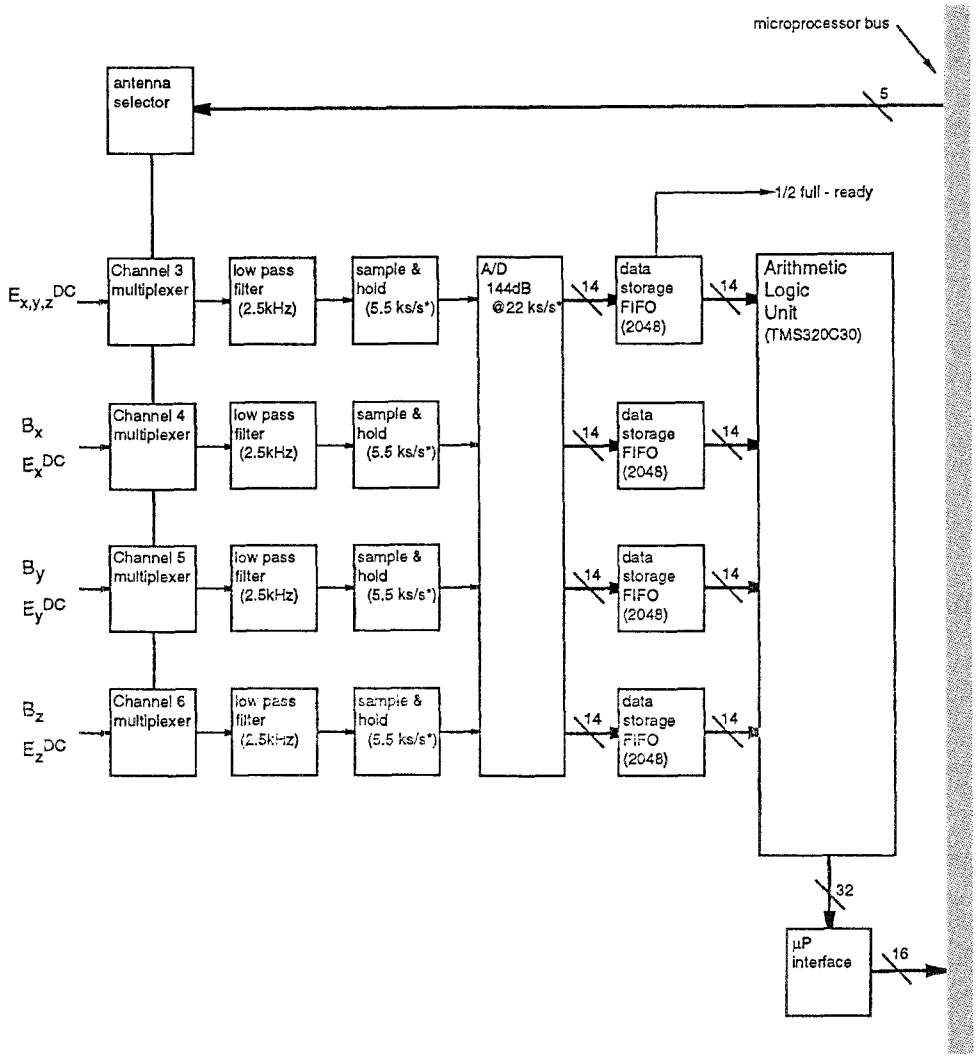

* sample rate = spin rate (spins/second) * 8 (sectors/spin) * 2 (FFT/sector) * 1024 (samples/FFT) + ε = 5,500 samples/second/channel

Fig. 3c. The FFT receiver. Mid band digitizers.

the DPU accumulating the average, peaks and phases for transmission to Earth at some appropriate telemetry rate. The telemetred values represent the average and peak power, in 1/2 dB steps; the phases are given relative to one channel in 22.5-deg steps. This system can thus give very flexible coverage of the entire spectrum with 100% duty cycle on all channels. Ground commands sent to the microprocessor controller will allow full programmable coverage of the entire spectrum while at the same time concentrating special interest on selected frequency bands. This flexibility allows fullest use of the available telemetry link.

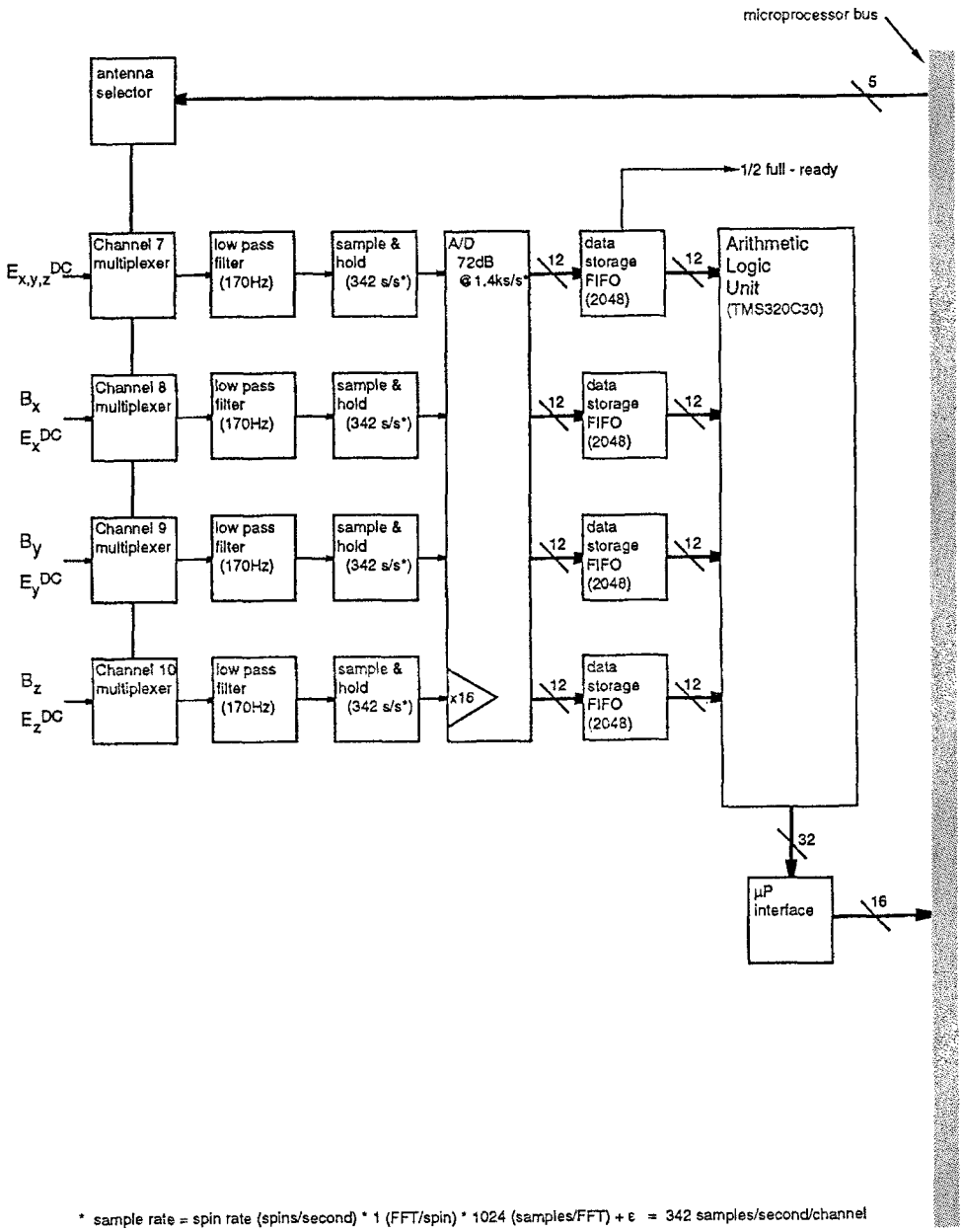

Fig. 3d. The FFT receiver. Low band digitizers.

For the two electric dipoles in the spin plane of the rotating WIND spacecraft, the variations of electric potential due to the variation of photoemission with area presented to the sun cause serious interference with low frequency measurements.

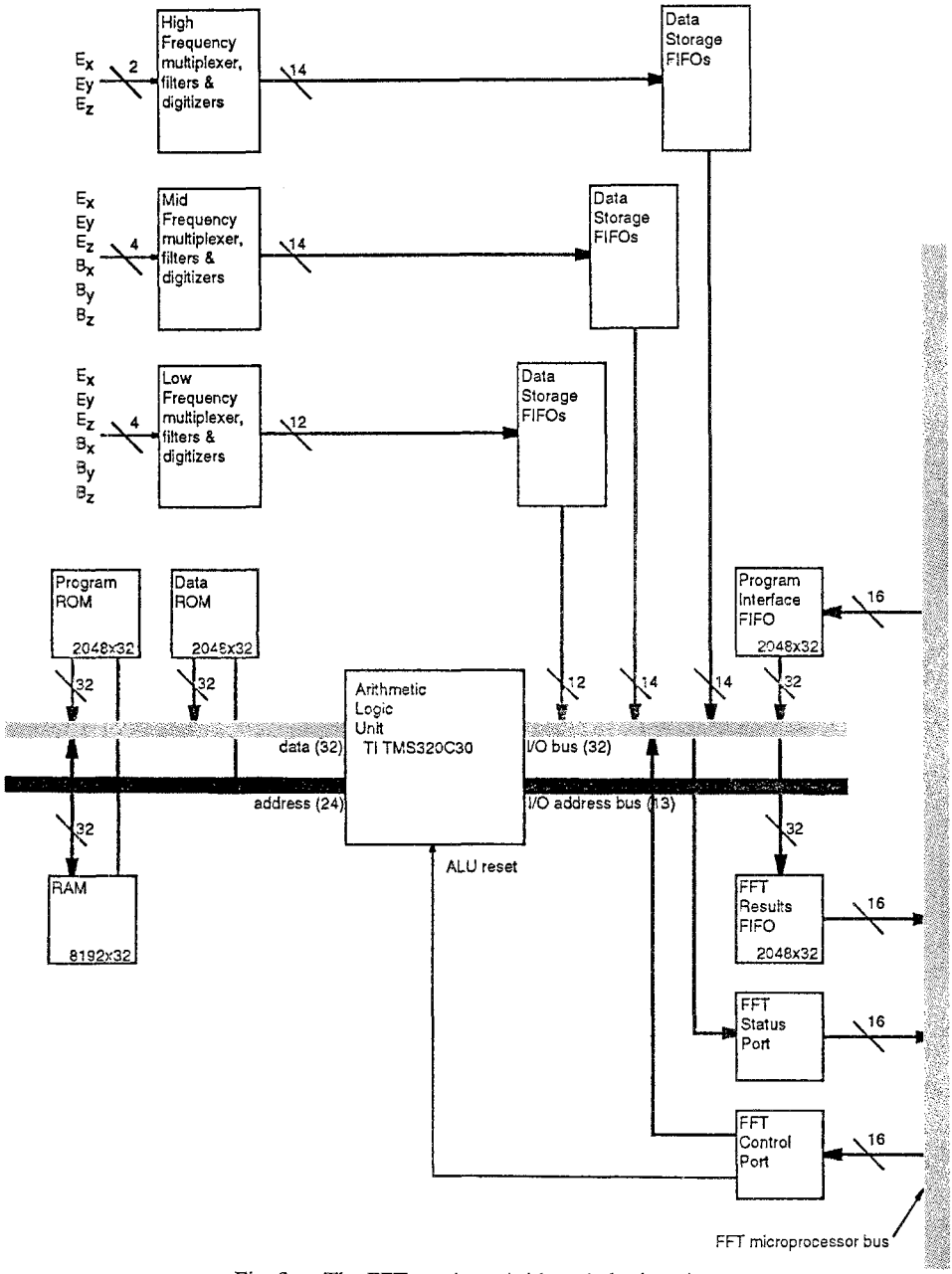

Fig. 3e. The FFT receiver. Arithmetic logic unit.

Such an antenna can be expected to change potential by 10 V or more in the shadow of the spacecraft or when it is pointing directly at the Sun. At the same time, because it has lost its photoelectron coupling to the plasma, the resistance between the antenna and the plasma rises, by a factor of about 10. We will attempt to

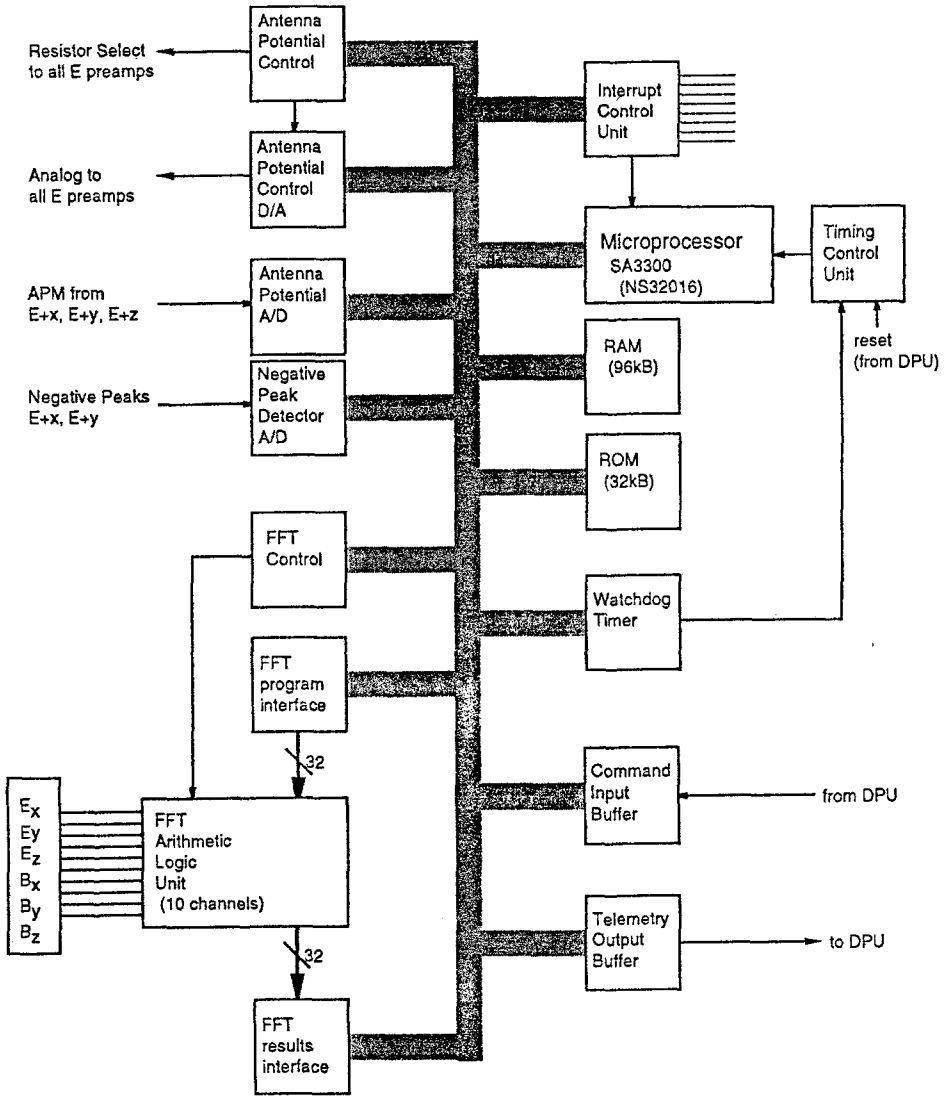

Fig. 3f. The FFT receiver. Microprocessor block diagram.

use this property to reduce the photoelectric variations of potential, and keep them within the linear range of the preamplifiers. To do this, each antenna is connected to a current source, consisting of a large resistor driven by a programmable voltage in the range from -10 to +10 V in 256 steps. The same resistors allow in-flight measurement of the antenna impedence.

The available resistor values are:

X	*Y*	*Z*
10 Meg	50 Meg	
100 Meg	500 Meg	
350 Meg	1500 Meg	
1000 Meg	10000 Meg	50 Meg

On orbit, the current source will be adjusted to have relatively little effect when the antenna is nearly perpendicular to the Sun and its resistance is low, and to provide electrons to replace photoelectrons when the antenna points toward or away from the Sun and its resistance is high.

3.4. THERMAL NOISE RECEIVER (TNR)

Two multi-channel receivers cover the frequency range of 4 kHz to 256 kHz in 5 logarithmically-spaced frequency bands. Each band covers 2 octaves with a 1 octave overlap. Each of these bands is divided into either 32 or 16 logarithmically-spaced channels. The block diagram of the TNR and the other (RAD1 and RAD2) receivers supplied by Meudon is shown in Figure 4.

The digital part of each receiver is preceded by an analog front end which provides anti-aliasing filtering and automatic gain control (AGC). The anti-aliasing filters are necessary to distinguish the signals below the Nyquist frequency from those above and are switched when the frequency band is changed. The AGC amplifiers 'normalize' the input to the digital receivers to an optimum value. The nominal allowable gain variation is 70 dB which, combined with the measurable variations within each band, provides for a total dynamic range in excess of 100 dB.

The digital filters were developed and used for the first time in the RETE experiment on the first Tethered Satellite System (TSS) mission. The principal characteristic of these receivers is their ability to operate at sampling frequencies above 1 MHz. Filters with upper frequency limits of more than 500 kHz are achievable. The filters are of the finite impulse response (FIR) type. Their coefficients have been determined by an optimization program and the maximum filter length are 512 or 256 taps. This results in passbands of 4.4% or 9% of the observed center frequency. The out-of-band rejections are greater than 45 dB, determined by the 8-bit digitization. 32 channels are calculated simultaneously in the nominal mode. The results of the calculations are hardware compressed into 8-bit words following a quasi-logarithmic law (average resolution 0.375 dB). This processing is equivalent to a wavelet transform analysis.

The basic measurement cycle has been determined by the time necessary to acquire enough information to reduce statistical variations to less than one quantization step (here 0.3 dB). It is nominally 20 ms for 1 MHz sampling, and is inversely proportional to the frequency band of interest. Table III shows the bandwidth for

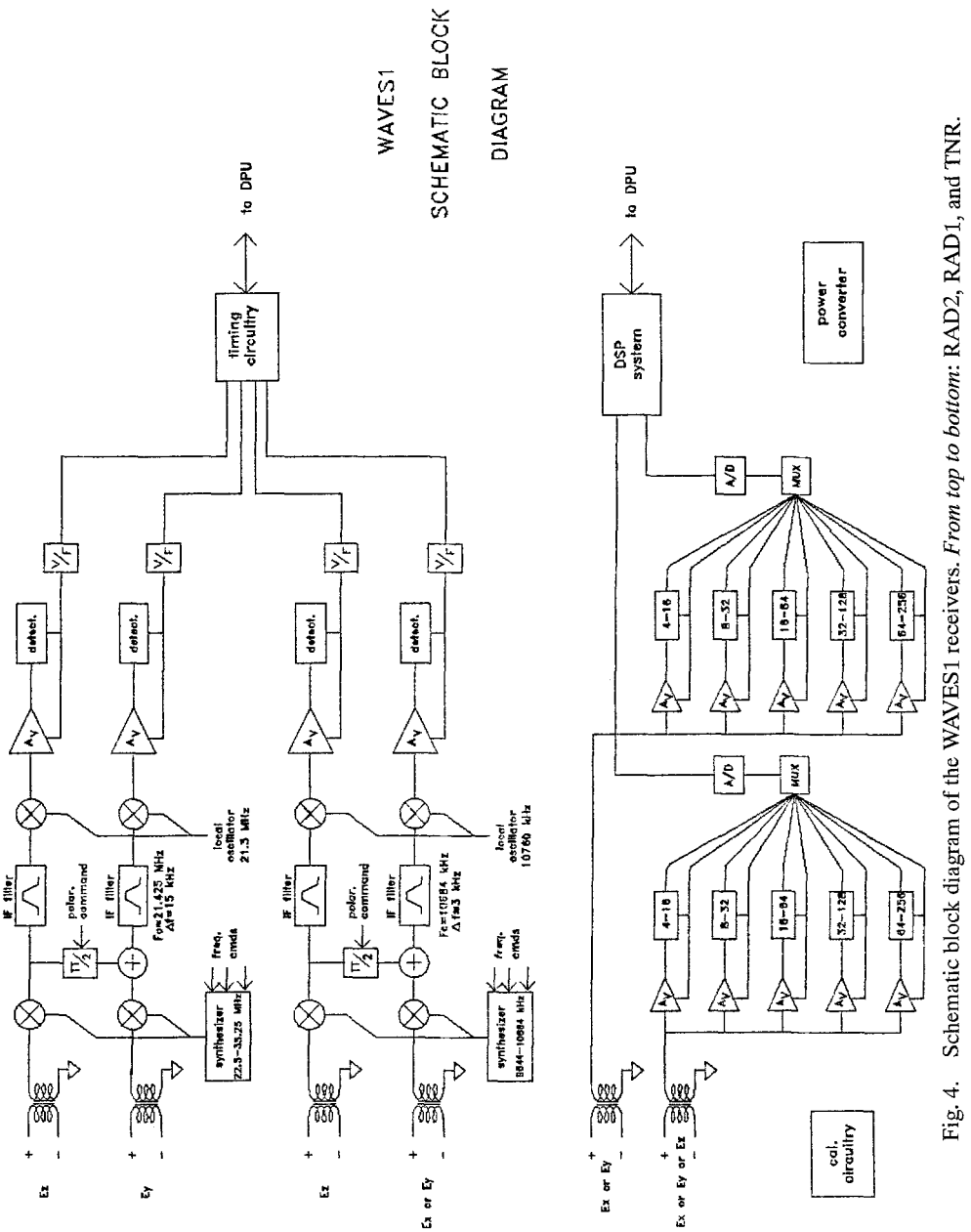

Fig. 4. Schematic block diagram of the WAVES1 receivers. *From top to bottom*: RAD2, RAD1, and TNR.

TABLE III
Characteristics of the thermal noise receiver (TNR)

Band	Range (kHz)	Sampling rate (kHz)	Measurement time (ms)
A	4–16	64.1	320
B	8–32	126.5	160
C	16–64	255.7	80
D	32–128	528.5	40
E	64–256	1000.	20

each of the 32 channels, the required sampling frequency and the measurement cycle for the various bands proposed. The considerable overlap in the frequency bands is intentional; this has been done so that there can be a 'tracking' of the characteristic plasma frequency, as will be discussed below.

In order to measure the low-frequency spectrum around the plasma frequency with the greatest frequency resolution it is desirable to stay within one optimized frequency band in which the plasma frequency is well situated. This is a principal operating mode of the TNR. However, this optimum frequency band is not known a priori because of the variability of the electron density.

The frequency range of observation (choice of one band among the 5 possible bands) can be decided by three different means. The first two means use real time determinations of the density moment obtained by two other investigations on the WIND spacecraft, namely the SWE low energy electron experiment and the 3D-PLASMA experiment. Therefore, in this mode, an estimate of the electron density (which is proportional to the plasma density) is made on-board on a medium time scale to select the correct band. The third means uses a neural network that recognizes and tracks the plasma line as it drifts in frequency, suggesting a band switching when necessary. The TNR passes the results of the neural network analysis to the DPU which uses a simple algorithm to select (keep or change) one frequency band among the five possible bands. This will be described in more detail in Section 4.3.

3.5. RADIO RECEIVER BAND 1 (RAD1)

The RAD1 dual radio receiver is essentially the same as that flying on the Ulysses mission. It consists of 2 super-heterodyne receivers operating in the 20–1040 kHz range. One is connected to the axial (E_z) electric dipole antenna, the other to a summation of the E_z antenna and either of the two spin plane antennas (E_x or E_y) (Figure 5). This is called the SUM mode. In what follows S stands for the sum of E_x (or E_y) and E_z with no phase shift, S' stands for the sum of E_x (or E_y) and E_z with a 90-deg phase shift, and Z is the measurement on the spin axis antenna.

The result of the summation (SUM mode) is to synthesize an inclined dipole. This configuration has been determined to be the optimum one for determination of the direction of arrival of received radiation on a spinning spacecraft. Using this technique (Manning and Fainberg, 1980; Fainberg *et al.*, 1985), the direction of the source centroid and its diameter can be determined as well as the 4 Stokes parameters. A SEP mode is also possible, where E_z and E_x are not summed.

The receiving frequency will be determined by a frequency synthesizer which in turn is driven by pre-determined observation programs either stored in PROM memory or uploaded by telecommand. These programs reside in the DPU. Some of these observation programs are designed to optimize the tracking of solar type III bursts, which implies smaller frequency increments along with slower sampling rates at the lower frequencies, other programs are suited for the analysis of kilometric radiation from the Earth and Jupiter. One program covers the same frequencies as the standard coverage of the Ulysses Radio Astronomy Receiver (RAR) (Stone *et al.*, 1992), in order to permit baseline measurements. Frequency tables and pointer lists are used. A frequency table generally consists of 16 observation frequencies selected among the 256 possibilities (4 kHz steps) provided by the synthesizer. A pointer list describes how each one of 16 arbitrary frequencies are scanned during a full cycle. A cycle generally consists of 64 steps. The pointer list points to numbers (0 to 15) in the frequency table. Both the frequency table and the pointer list can be independently selected via telecommand and both can be modified in flight.

The bandpass of the receivers is 3 kHz, determined by crystal filters in the IF amplifiers at 10.7 MHz. The acquisition time for one individual measurement is 0.154 s, determined by the IF bandpass and by the time necessary to reduce statistical fluctuation to below the quantization value (about 0.35 dB). Table IV shows the main characteristics of both RAD1 and RAD2.

3.6. Radio Receiver Band 2 (RAD2)

This dual receiver is very similar to the RAD1 receiver except that the frequency range is much higher (see Table IV). The band covered is 1.075 to 13.825 MHz. The receiver uses only the shorter (E_y) antenna system because the longer antennas are not usable above their full-wave resonance of about 3.3 MHz. The bandpass of these receivers is 20 kHz, determined by crystal filters at the IF frequency of 21.425 MHz. The frequency step increment is 50 kHz. The acquisition time is 20 ms, which also must take into account the time necessary for synthesizer switching and stabilizing. Observation programs are similar to but more complex than those used for RAD1 but are designed to take advantage of the RAD2 frequency range.

3.7. Time Domain Sampler (TDS)

The Time Domain Sampler (Figure 6) will be used to gather fast waveform data directly from the electric antennas and the search coils as well as extending the

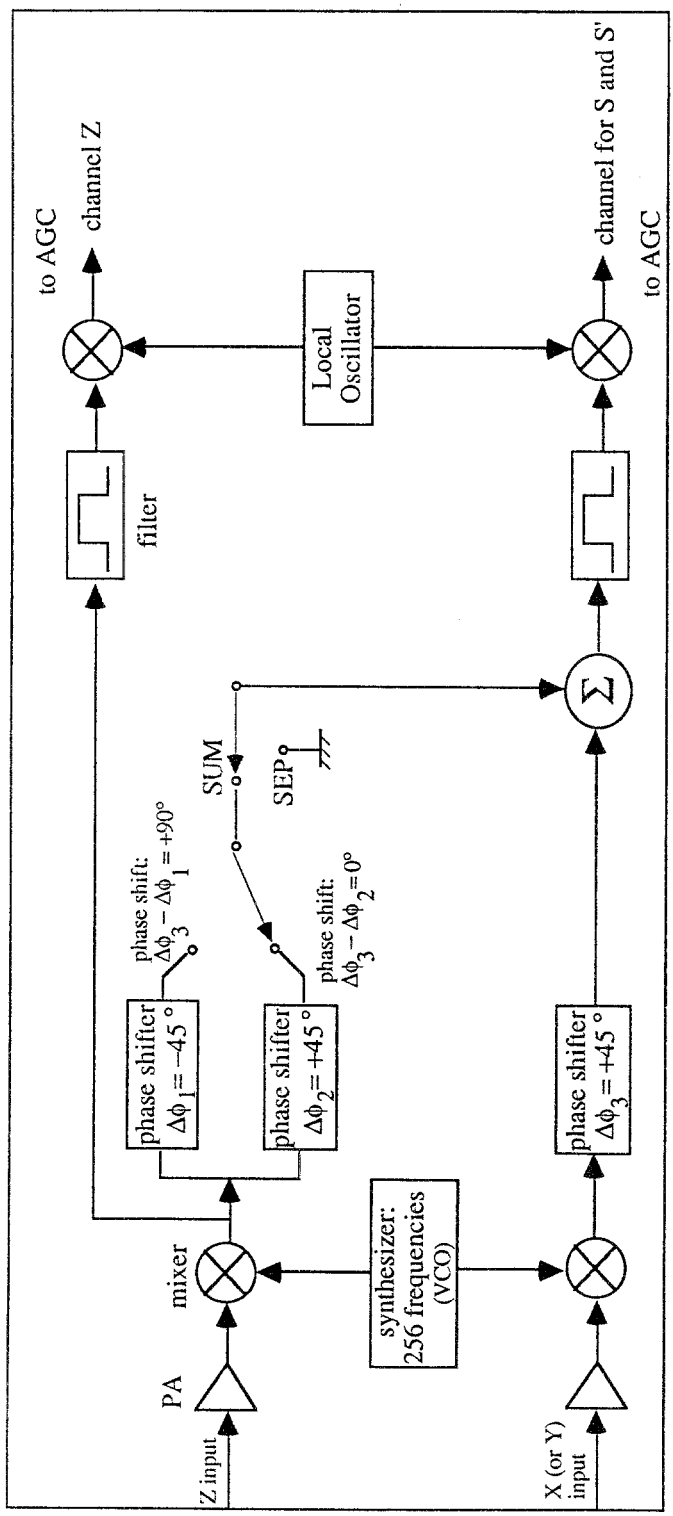

Fig. 5. Block diagram of the receiver system designed to determine the angular and polarization properties of the low-frequency radio sources measured from a spinning spacecraft.

TABLE IV
Main characteristics of the radio receivers

	RAD1	RAD2
Frequency span	20 kHz–1040 kHz	1.075–13.825 MHz
Number of frequencies	256	256
Frequency step	4 kHz	50 kHz
Filter		
nominal 3 dB BW	3 kHz	20 kHz
effective noise BW	3.4 kHz	19 kHz
Acquisition time for a set of S, S', Z	358 ms	63 ms
Number of sets measured per freq. per spin	$8S + 8S' + 8Z$	$12S + 12S' + 12Z$
Number of frequencies measured per spin	1	4
Number of steps per standard cycle	64	48
Duration of standard cycle	192 s	36 s

lower limit of frequency coverage to 0.03 Hz, below the lower limit of the FFT (0.3 Hz). Data will be digitized over a wide dynamic range at a top speed of 120 ksamples per second (ksps). The fast sampler part of the TDS allows sampling of two channels at as many as 120 ksps while the slow sampler allows sampling at up to 7.5 ksps. Table V shows the possible sampling rates.

The sampling rate is programmable by ground command as is the selection of anti-aliasing low pass filters. After passing through the low pass filters, the data from the fast or slow samplers are simultaneously sampled and digitized with a logarithmic converter giving 90 dB of dynamic range.

Hardware comparators in both the fast and slow samplers detect peak absolute values and, using a shift register, arrange the data in a large (2048 byte/channel) section of memory with the peak value in the center of the recorded event. The TDS microprocessor is alerted when a full event is gathered.

Because the TDS has an overall peak sampling rate of over 2 Mbits s^{-1} and a typical telemetry rate of only 15 bits s^{-1}, something must be done to reduce the amount of TDS data sent to the ground. It is especially important not to waste bit-rate with spurious events such as switch closures or thruster firings. To this end, an intelligent mechanism has been developed to reduce the number of 'uninteresting' TDS events which are sent to the ground. After collecting an event, the processor invokes a ground loadable neural network to assign a quality for the new event. When there is room in the WAVES telemetry stream for TDS data, the highest quality event will be packetized and transmitted. A neural network has been implemented that will learn to select events according to criteria that will be adjusted after getting the results of the first observations. Additional measures will be taken to compress the data in order to save telemetery space.

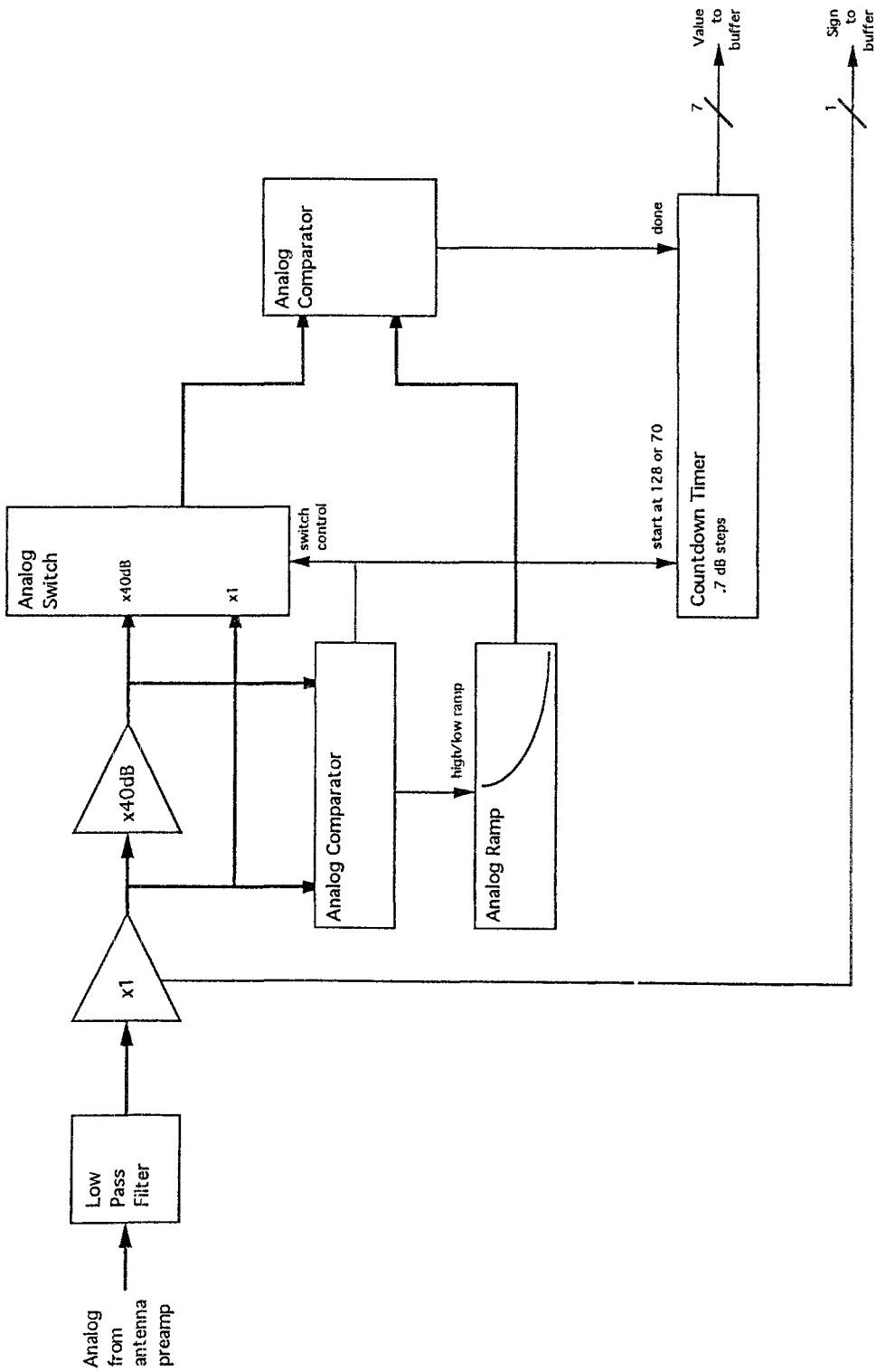

Fig. 6a. The TDS receiver. 90 dB logarithmic analog to digital converter.

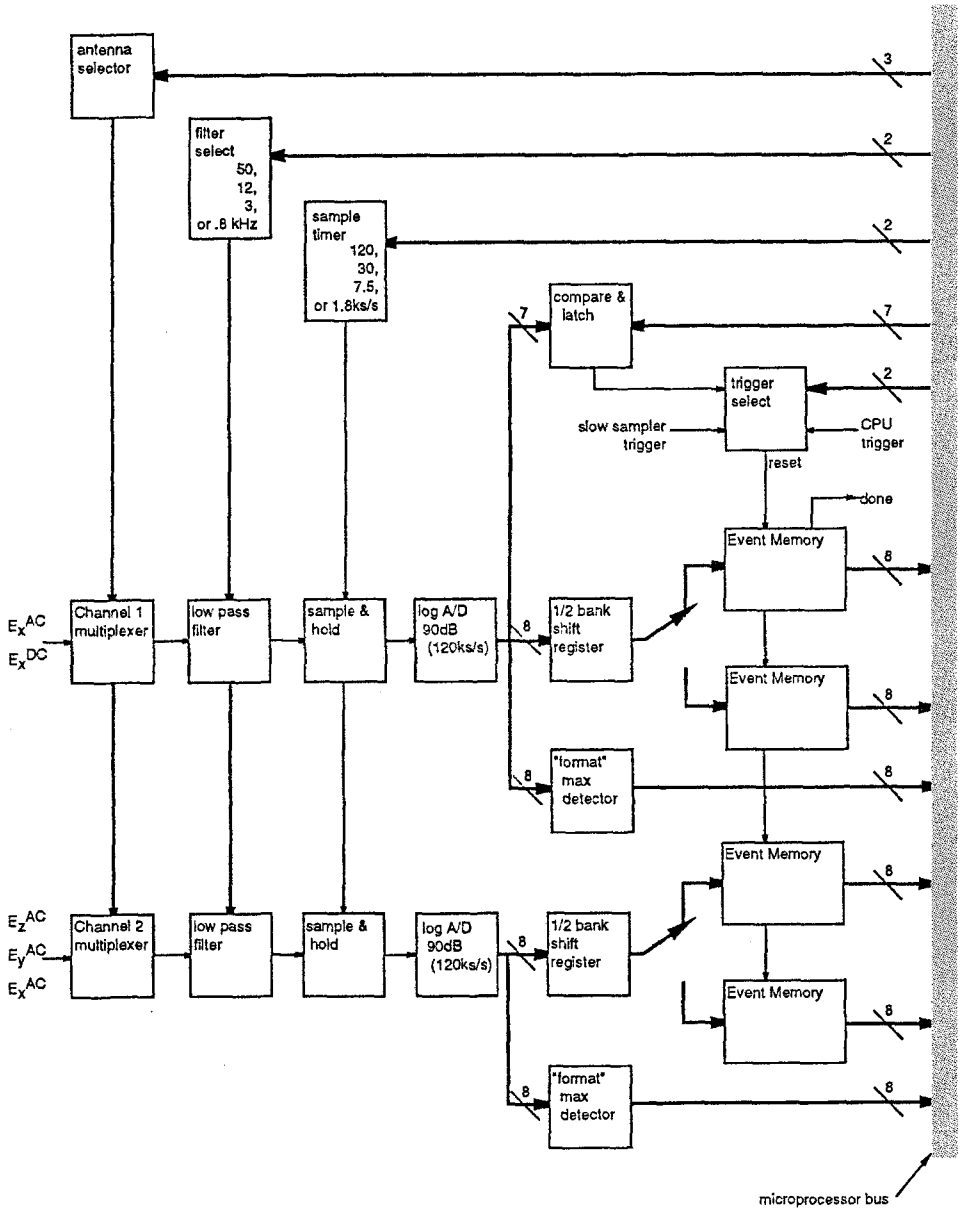

Fig. 6b. The TDS receiver. Fast sampler.

In addition to the high speed sampling of the TDS, WAVES also produces some low speed science. Once each spacecraft major frame (46 s in high bit rate and 92 s in low bit rate) an array of scientific as well as housekeeping measurements are made. While acquiring data at very high speeds, the TDS hardware also records the largest values (in absolute value) observed on all six of its channels. These peak

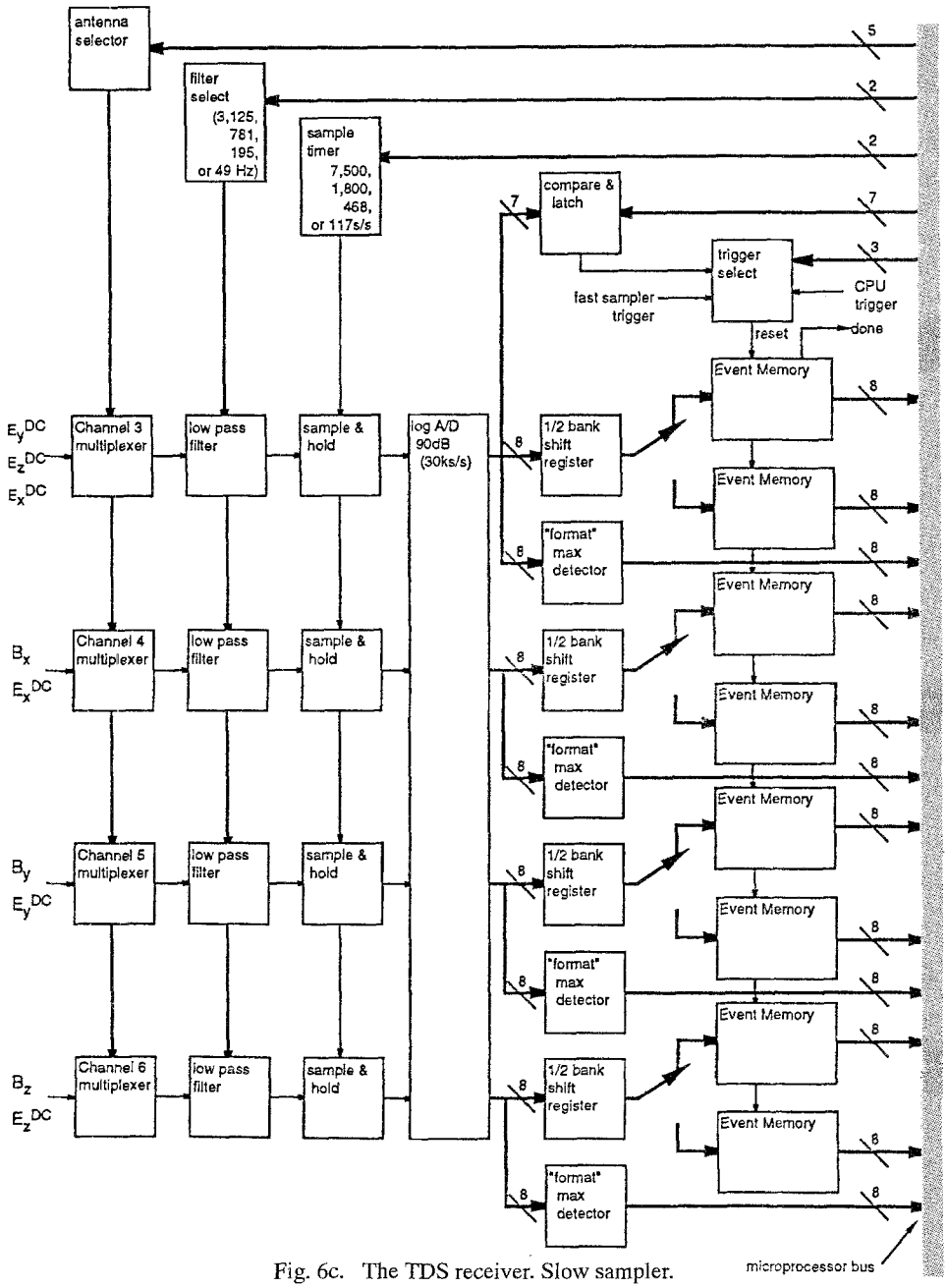

Fig. 6c. The TDS receiver. Slow sampler.

values are sent to telemetry once each major frame providing a coarse overview of transient activity.

In order to continuously monitor the antenna potential of the electric dipoles, one sample is taken from each of three orthogonal monopoles at a programmable

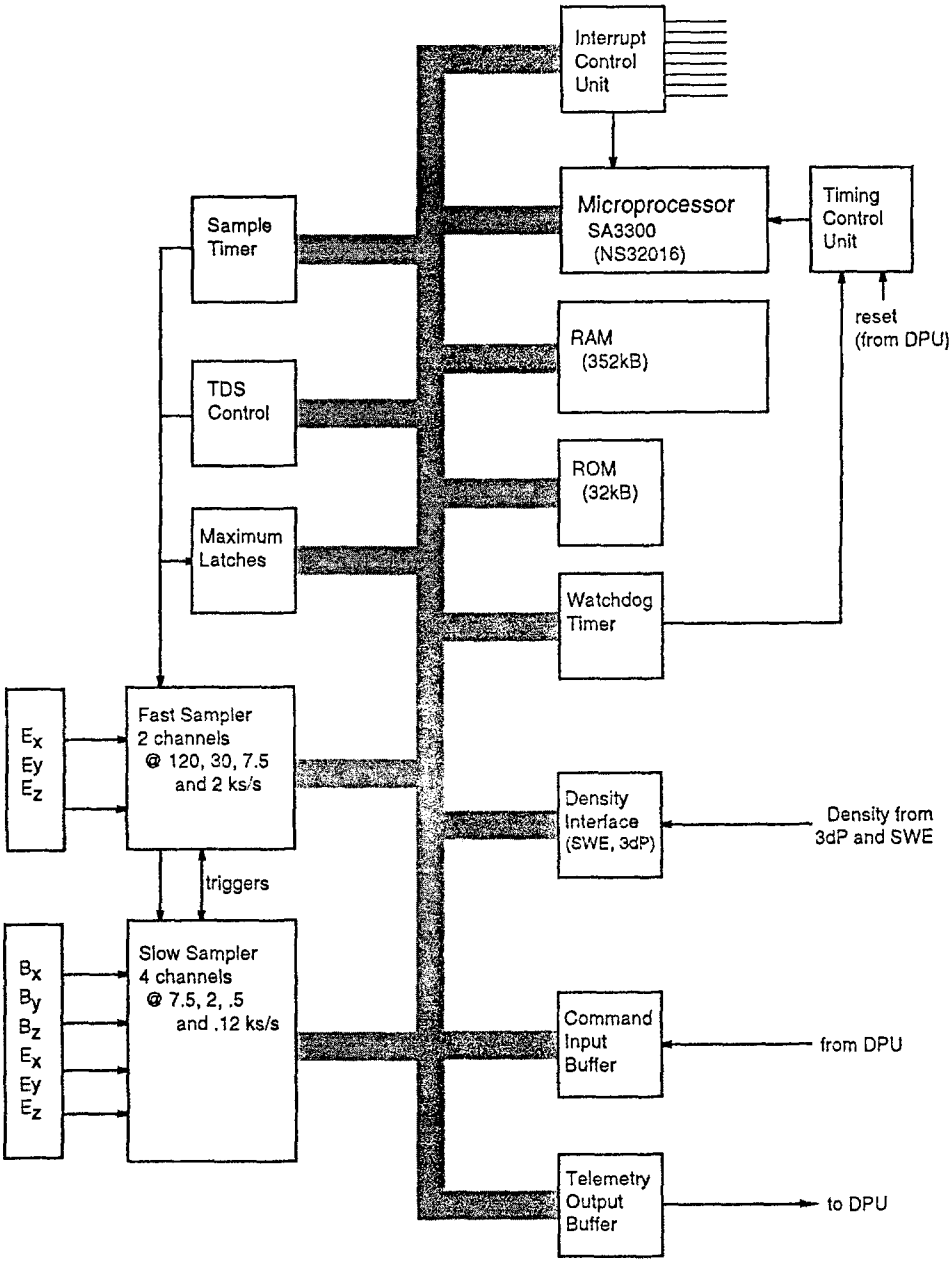

Fig. 6d. The TDS receiver. Microprocessor block diagram.

solar reference angle. One set of measurements is made and sent to the telemetry stream each major frame. In addition, the largest value observed during a spacecraft spin period (3 s) is latched and sent to telemetry once per major frame.

TABLE V
Possible sampling rates of the TDS

Speed	Fast sampler (sps)	Slow sampler (sps)
A	120,000	
B	30,000	
C	7,500	7,500
D	1,800	1,800
E		468
F		117

3.8. DC/DC POWER CONVERTER

The DC/DC power converter is very similar to that which was developed for the URAP experiment on the Ulysses spacecraft. The EMI emissions of this converter is extremely low. The converter is designed such that no single failure will cause loss of the entire WAVES instrument. Separate output stages (choppers, tranformer, filters) are used for major components of the instrument:

- electric preamplifiers,
- TNR, RAD1, RAD2,
- FFT, TDS and search coils,
- DPU.

In addition, the output stage for the DPU is redundant. The input stages and the oscillators are redundant, each of the 2 parts being capable of performing the total task.

The converter is located in the stack containing the Meudon electronics.

3.9. ELECTROMAGNETIC AND ELECTROSTATIC CLEANLINESS

EMC (Electromagnetic Cleanliness)

Many of the WAVES scientific objectives are based on the measurement of low level signals, for which all of the designed sensitivity is required. For instance, this is the case for the TNR measurements, for which the signal strength is quite low. It has been shown that these mesurements are feasible in the case of 'electrically clean' satellites, such as ISEE-3/ICE and ULYSSES.

A number of measures have been taken in collaboration with the Project and the spacecraft manufacterer to insure this capability on WIND (and POLAR):

- Early in the project an EMC commitee was formed to have oversight on all aspects of the spacecraft development and testing.
- A coherent and proper grounding and cable shielding philosophy was defined and imposed on the spacecraft and experiments.

– A frequency control plan was established to limit power converter frequencies to narrow bands (no variable frequency oscillators were allowed).

– Discussions with subsystem and instrument developers were undertaken to assist in good EMC design.

– Subsystem-level EMC test results were reviewed and exceedances of specifications were studied and judgement was made as to whether or not remedial actions were required.

– An excellent system-level EMC test was performed in a large enclosed EMC chamber with the spacecraft mounted on a wooden mount.

Some design incompatibilities, mainly in the instruments, were resolved by compromise and best engineering judgement. For instance, in a number of cases it was preferred not to impose a classic single-point ground philosophy which could have resulted in electrically isolating an instrument chassis, but rather to ground the box and limit current paths between the subsystem grounds.

This system-level test was very succesful and demonstrated the effectiveness of the generally simple but well-conceived EMC efforts. With a few identified exceptions the spacecraft was determined to be exceptionally 'clean', and the few noted problems have been resolved.

ESC (Electrostatic Cleanliness)

The maintenance of the spacecraft as a surface that is nearly equipotential is essential for DC and very low frequency electric field measurements. This requirement is also very important for the low-energy partcle experiments and we have cooperated with them in assisting in the overall spacecraft design as part of the EMC committee's goals. We believe that these goals have been completed but there is no way of testing this on the ground before launch.

4. On Board Data Processing

4.1. Data Processing Unit (DPU)

The DPU functions as the master processor for the WAVES experiment. A block diagram is shown in Figure 7. Its functions are:

(1) receive telecommands from the spacecraft;
(2) send telemetry to the spacecraft;
(3) control and acquire data from the TNR;
(4) determine optimum TNR frequency range;
(5) control and acquire data from the RAD1;
(6) control and acquire data from the RAD2;
(7) pass commands to and telemetry from the TDS;
(8) pass commands to and telemetry from the FFT;
(9) send housekeeping information to telemetry.

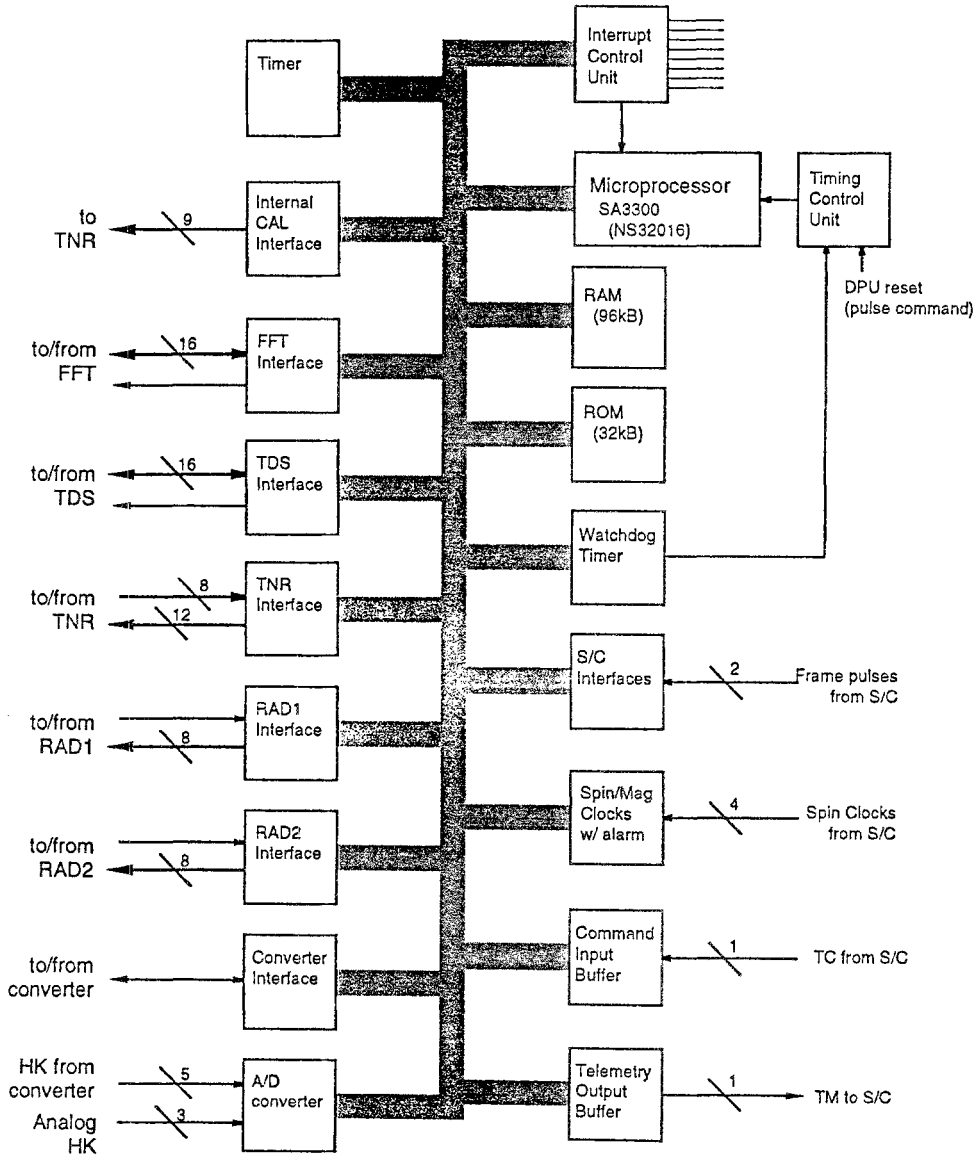

Fig. 7. The DPU microprocessor block diagram.

The WAVES team has chosen the Sandia SA3300 implementation of the National Semiconductor 32016 CPU for use in the parts of its instruments that contain a microprocessor (the DPU, TDS and FFT). This microprocessor offers both power and simplicity of programming. Specialized digital signal processors, the TMS320C30 and ADSP2100, are also used in the FFT and the TNR respectively.

All WAVES flight software is designed such that virtually any software module can be replaced in flight by a memory load telecommand. This design will make it possible to modify the flight software as scientific or practical needs dictate.

TABLE VI
Default waves packet allocation

	Low-bit rate	High-bit rate
RAD 1	8%	4%
RAD2	40%	20%
TNR	25%	25%
FFT	25%	45%
TDS	2%	6%

The WAVES investigation makes use of a packetized telemetry. Packetized telemetry offers flexibility both in flight and in ground data handling unavailable in a 'fixed format' telemetry system. The WAVES team has implemented their own form of packetized telemetry using the words allocated to the experiment within the fixed telemetry frames. As such, WAVES can dynamically alter telemetry allocations among the various WAVES subsystems (e.g., RAD1, RAD2, FFT).

4.2. Operational Modes

A standard survey rate of 936 bps (low bit rate) will be used within which the basic science investigations are performed. The built-in flexibility of the instrument and its DPU is such that the data rate of each instrument subsystem can be modified easily and the overall instrument data rate can be changed (increased) very readily in case of changing availability of telemetry.

During the standard survey rate the data format will be variable; the internal DPU will perform a 'packetizing' of the data from the different parts of the experiment in different regions of scientific interest. Table VI gives the default WAVES packet allocation for the two telemetry bit-rates.

4.3. Use of Neural Networks in Real-Time

Neural networks will be used in the WAVES instrument to perform instrument control for the TNR and data selection functions for the TDS. In both cases, the network, which is embedded in the flight software, is a feed-forward, back propagation algorithm that has been transformed into the integer domain for speed of processing – using lookup tables rather than computing continuous functions. The network coefficients are generated in the real-valued domain on the ground, transformed into integers, and can then be uploaded to the instrument during the mission to refine the selection algorithm as experience and data are acquired. Indeed, if there is cause, special coefficient tables can be developed to answer other types of questions, or recognize different phenomena.

For the TNR, we determined the ROM coefficient set from Ulysses Radio Receiver (RAR) data, processed to resemble the response of the WIND TNR

receiver. Using this data set, simulations demonstrate that the channel containing the thermal plasma line can be determined exactly about 85% of the time and within ± 1 TNR channel more than 99% of the time. While this recognition rate is unlikely to be equalled in flight with the RAR coefficient set, early data will be used to create a new set and recognition rates should become comparable. The neural network output can be used either alone or in concert with other plasma line indications from SWE and 3D-PLASMA to determine whether a different TNR band should be selected. The neural network estimates the peak frequency at real time rates so the peak can be followed when it moves quickly in frequency e.g., due to shock activity. In the TNR fast mode, the neural network peak finding capability performs intelligent selection of the points to be telemetered so that, even with a fraction of the spectral coverage, the plasma characteristics can still be resolved accurately. In this mode, it is expected to obtain about 4 measurements of the electron density per half spacecraft spin (1.5 s). In order to avoid being mislead by the neural network results, a programmable 'honesty' factor causes the TNR to sweep through the five frequency bands periodically.

For the TDS, simulations with rocket data indicate that a neural network can be used to select the time series that contains a given signature. Because the TDS samples at a rate several orders of magnitude higher than its telemetry allocation, an intelligent selection functions optimizes telemetry use by selecting the 'best' candidate event. The neural net is trained to recognize event signatures, and distinguish them from spurious triggers or signatures that are not required, while simultaneously ranking them according to the degree to which they resemble the paradigm signature. As the mission evolves, the desired signatures may change, and new coefficient tables will be transmitted accordingly. The software and coefficient tables will be uploaded to RAM after launch once coefficients are determined using in-flight experiment data, since only then will a suitable dataset be available. To maintain integrity, the instrument will sometimes choose TDS events without regard for the neural network quality.

4.4. INTER-EXPERIMENT INTERFACES

Three inter-experiment interfaces have been implemented:

– N_e signal from the SWE experiment. This will take the form of a single serial data line from the Plasma experiment to the WAVES experiment. Every fixed period, the Plasma Experiment sends a serially encoded number representing the local electron density. The WAVES experiment uses this number as an aid in setting the frequency range of the TNR.

– N_e signal from the 3D-PLASMA experiment. This will be similar to the interface to the SWE experiment.

- E_x and E_y signals to the 3D-PLASMA experiment for wave/particle correlation studies. These are analog signals from the mid-frequency preamp outputs.

The 3D-PLASMA correlator then performs a one bit cross-correlation between the field signals and the particle counts.

5. Calibrations

The calibrations yield the receivers' responses and permit to convert the binary telemetry data received on the ground into the physical parameter measured by the sensors. They are done at the laboratory before launch (ground calibrations) and also during the mission (in flight calibration): the instrument includes an internal noise generator which allows one to check periodically this response and to monitor any change in the receiver characteristics.

Ground calibrations

Very sophisticated and precise test equipment has been designed and built for testing the instrument on the ground. Sinewave and white-noise sources are provided. The instrument underwent final calibrations during the instrument refurbishment period in October–December 1993 at the University of Minnesota. At that time important secondary parameters such as antenna mechanism and preamplifier stray input capacitance were carefully measured. We believe that the receiver transfer characteristics have been determined to accuracies of 2 to 10% depending on the receivers and that the stray capacitances are known to within 1 pF for the wire antennas (40 ± 1 pF) and 3 pF for the axial booms (88 ± 3 pF).

The noise generator used for ground calibrations is a pseudo-random noise generator. It gives seven different frequency bands.

For the RAD1 and RAD2 receivers, 3 kinds of test have been completed:

(1) A gain curve measurement for each receiver ('log law').

(2) A frequency response measurement (bandwidth) for each receiver.
Different configurations have been tested:

S and Z:
– SEP mode, signal on X or Y and Z, output signal readout on channels
– SUM mode, signal on X or Y and Z, output signal readout on channels

S, S', and Z:
– SUM mode, signal on Z only, output signal readout on channel S, S'.
– SEP mode, signal on Z only, output signal readout on channel S and *vice versa* (diaphony measurements).

(3) Phase measurements: they allow to calibrate the 0 deg and the 90 deg of the phase shifters.

For the TNR receiver, 2 kinds of test have been completed:
(1) A gain curve measurement for the receiver ('log law').
(2) A frequency response measurement (bandwidth).
The 0 dB of the noise generator has also been calibrated.

The gain curve response of the receivers can be mathematically modelled by the following 'log law':

$$y = A_2 \log 10[(10^{(A_1 - x)/10} + 10^{-A4)^{1/4} - 1)} + A_3 \, .$$

The coefficients A_1, A_2, A_3, A_4 are the calibration parameters to be computed by numerical fitting. These coefficients have a physical significance in the AGC circuitry: gains, offsets, etc., which can yield detailed information on the time evolution, if any, of the characteristics of the receivers.

In Flight Calibrations
For low-frequency electric field measurements, it is necessary to know the effective resistance of the electric antennas to the spacecraft and to the plasma. This will be done by periodically switching in a set of the same resistances and source voltages that are used by the antenna potential control system, and measuring the effect of the consequent antenna loading on the DC electric field of the solar wind. The loading effect will be measured by the antenna potential monitor (+ antennas only) and by the low frequency channel of the FFT (difference between antennas).

The magnetic search coils are equipped with calibration windings which may be computer controlled to provide low frequency calibration signals.

For the RAD1, RAD2 and TNR receivers, an internal noise generator provides 8 attenuation levels (8 dB steps), applied successively to the receiver inputs (after the preamplifiers) for the 8 levels and at the input of the IF stages for only one level. The internal calibration cycle which allows us to check the stability of the receivers and to correct the calibration curves used during the data analysis is automatically performed during the mission at regular intervals (e.g., every 24 hours) or can be initiated by telecommand.

6. Conclusions

The WAVES investigation on the WIND spacecraft uses state-of-the-art techniques to explore in a new way the radio and plasma wave phenomena in Geospace and in the interplanetary medium, down to the solar wind acceleration regions. The main science objectives are summarized below.

Geospace Science
To monitor the state of the solar wind as it approaches the Earth; to study the solar wind/Geospace couplings, to analyze the heat flux and anisotropies in different

regions and through different boundaries of Geospace; to study the Earth's bow shock including upstream waves.

Solar/Interplanetary Science
To study the source region of the solar wind; to map large scale interplanetary structures; to analyze stream interactions; to study impulsive phenomena (flare related particle streams, long duration (10 days or more) particle streams, interplanetary shock formation and acceleration).

Plasma Physics
To study a very broad range of phenomena relating to instabilities, waves and turbulence and to basic radiation mechanisms.

Achieving all this will require as broad a collaboration as possible, essentially within the Global Geospace Science Initiative and also with the International Solar Terrestrial Physics Program. For instance detailed collaborative programs already exist with the ULYSSES program (for which WAVES will provide the ecliptic plane reference for radio pheneomena), and the LASCO and EIT investigations on the SOHO spacecraft which will cover common volumes of the solar corona and interplanetary medium, but will use different types of remote diagnosis.

Acknowledgements

Eight different institutions have contributed to the WAVES investigation, in four different countries: France, the U.S.A., Ireland and Greece. We wish to thank for their contributions scientists, engineers and technicians who have contributed, in one way or another to this program. This includes at DESPA: D. Carrière, J.-P. Mengué, C. Guériau, C. C. Harvey (co-investigator), R. Hulin, R. Knoll, C. Lacombe (co-investigator), N. Meyer-Vernet, G. Nicol, M. Poquérusse (co-investigator), J.-L. Steinberg (co-investigator), F. Wouters, and P. Richaume (who contributed to the development of the Neural Networks for TNR); at DAEC, Observatoire de Meudon: L. Celnikier; at the University of Minnesota: J. Kappler, R. L. Howard, L. Wiesensel, S. Ring, A. Knutson; at the University of Iowa: D. A. Gurnett (co-investigator), and D. Odem; at Goddard Space Flight Center: J. Fainberg (co-investigator) and M. Reiner (Hughes STX) who have both actively contributed to the instrument calibration, R. G. Stone (co-investigator), M. Desch, R. J. MacDowall, and F. Grena; at St. Patrick's College, Maynooth, Ireland: S. McKenna-Lawlor (co-investigator), and R. Reilly (STIL); at the University of Athens: C. Caroubalos (co-investigator); at the Naval Research Laboratory, Washington, D.C.: R. Howard and P. Rodriguez (co-investigators); at Jet Propulsion Laboratory: E. J. Smith (co-investigator). Not to forget the numerous persons on the GGS Project at Goddard and the Martin-Marietta East-Windsor plant, among which: E. Werner, R. Harten, D. Riley, T. Palumbo, and A. Munro.

Finally, the authors wish to thank the referees for their detailed comments and recommendations that have led to significant improvements on the manuscript.

References

Bougeret, J.-L., Fainberg, J., and Stone, R. G.: 1983, 'Determining the Solar Wind Speed Above Active Regions Using Remote Radio Wave Observations', *Science* **222**, 506.

Bougeret, J.-L., Fainberg, J., and Stone, R. G.: 1984, 'Interplanetary Radio Storms: 1. Extension of Solar Active Regions Through the Interplanetary Medium', *Astron. Astrophys.* **136**, 255.

Burgess, D., Harvey, C. C., Steinberg, J.-L., and Lacombe, C.: 1987, 'Simultaneous Observation of Fundamental and Second Harmonic Radio Emission from the Terrestrial Foreshock', *Nature* **330**, 732.

Canu, P.: 1990, 'Oblique Broadband Electron Plasma Waves Above the Plasma Frequency in the Electron Foreshock: 1990', *J. Geophys. Res.* **95**, 11,983.

Fainberg, J., Hoang, S., and Manning, R.: 1985, 'Measurements of Distributed Polarized Radio Sources from Spinning Spacecraft; Effect of a Tilted Axial Antenna. ISEE-3 Application and Results', *Astron. Astrophys.* **153**, 145.

Gurnett, D. A.: 1974, 'The Earth as a Radio Source: Terrestrial Kilometric Radiation', *J. Geophys. Res.* **79**, 4227.

Gurnett, D. A.: 1975, 'The Earth as a Radio Source: the Non-Thermal Continuum', *J. Geophys. Res.* **80**, 2751.

Hoang, S., Dulk, G. A., and Leblanc, Y.: 1994, 'Interplanetary Type III Radio Bursts that Approach the Plasma Frequency: Ulysses Observations', *Astron.Astrophys.*, in press.

Lacombe, C., Mangeney, A., Harvey, C. C., and Scudder, J. D.: 1985, 'Electron Plasma Waves Upstream of the Earth's Bow Shock', *J. Geophys. Res.* **90**, 73.

Lacombe, C., Harvey, C. C., Hoang, S., Mangeney, A., Steinberg, J.-L., and Burgess, D.: 1988, 'ISEE Observations of Radiation at Twice the Solar Wind Plasma Frequency', *Ann. Geophysicae* **6**, 113.

Manning, R. and Fainberg, J.: 1980, 'A New Method of Measuring Radio Source Parameters of a Partially Polarized Distributed Source from Spacecraft Observations', *Space Sci. Inst.* **5**, 161.

Maroulis, D., Dumas, G., Bougeret, J.-L., Caroubalos, C., and Poquerusse, M.: 1993, 'The Digital System ARTEMIS for Real-Time Processing of Radio Transient Emissions in the Solar Corona', *Solar Phys.* **147**, 359.

Meyer-Vernet, N. and Perche, C.: 1989, 'Tool Kit for Antennae and Thermal Noise Near the Plasma Frequency', *J. Geophys. Res.* **94**, 2405.

Reiner, M. J., Fainberg, J., Stone, R. G., Kaiser, M. L., Desch, M. D., Manning, R., Zarka, P., and Pedersen, B. M.: 1993, 'Source Characteristics of Jovian Narrow-Band Kilometric Radio Emission', *J. Geophys. Res.* **98**, 13,163.

Steinberg, J.-L., Hoang, S., and Bosqued, J.-M.: 1990, 'Isotropic Terrestrial Kilometric Radiation: a New Component of the Earth's Radio Emission', *Ann. Geophysicae* **8**, 671.

Stone, R. G. and 31 co-authors: 1992, 'The Unified Radio and Plasma Wave Investigation', *Astron. Astrophys. Suppl. Ser.* **92**, 291.